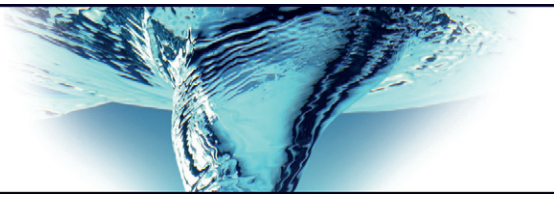
J. Fluid Mech. (2014), *vol.* 743, R1, doi:10.1017/jfm.2014.73



JFM RAPIDS
journals.cambridge.org/rapids

Sharp transition between coalescence and non-coalescence of sessile drops

Stefan Karpitschka† and Hans Riegler

Max Planck Institute of Colloids and Interfaces, 14424 Potsdam, Germany

(Received 13 December 2013; revised 16 January 2014; accepted 31 January 2014;
first published online 4 March 2014)

Unexpectedly, under certain conditions, sessile drops from different but completely miscible liquids do *not* always coalesce instantaneously upon contact: the drop bodies remain separated in a temporary state of *non-coalescence*, connected through a thin liquid bridge. Here we investigate the *transition* between the states of instantaneous coalescence and temporary non-coalescence. Experiments reveal that it is barely influenced by viscosities and absolute surface tensions. The main system control parameters for the transition are the arithmetic means of the three-phase angles, $\overline{\Theta}_a$, and the surface tension differences $\Delta\gamma$ between the two liquids. These relevant parameters can be combined into a single system parameter, a specific Marangoni number $\widetilde{M} = 3\Delta\gamma/(2\overline{\gamma}\overline{\Theta}_a^2)$. This $\widetilde{M}$ universally characterizes the coalescence transition behaviour as a function of both the physicochemical liquid properties and the shape of the liquid body in the contact region. The transition occurs at a certain threshold value $\widetilde{M}_t$ and is sharp within the experimental resolution. The experimentally observed threshold value of $\widetilde{M}_t \approx 2$ agrees quantitatively with values obtained by simulations assuming realistic material parameters. The simulations indicate that the absolute value of $\widetilde{M}_t$ very weakly depends on the molecular diffusivity.

Key words: breakup/coalescence, convection, drops and bubbles, interfacial flows (free surface), marangoni convection, thin films

1. Introduction

Sessile drops of identical liquids spreading on a shared substrate will coalesce immediately after coming into contact. The driving mechanism for drop coalescence is capillarity. Recently, details of the coalescence behaviour of sessile drops have also been the focus of fundamental research (Ristenpart *et al.* 2006; Borcia, Borcia & Bestehorn 2012; Hernandez-Sanchez *et al.* 2012; Castrejón-Pita *et al.* 2013; Eddi, Winkels & Snoeijer 2013). This is, not least, motivated by new applications e.g. ink-jet

† Email address for correspondence: Stefan.Karpitschka@mpikg.mpg.de

© Cambridge University Press 2014

https://doi.org/10.1017/jfm.2014.73 Published online by Cambridge University Press

printing (Ihnen *et al.* 2012; Hanyak, Darhuber & Ren 2011; Stringer & Derby 2010) or microfluidics (Christopher *et al.* 2009; Li *et al.* 2011).

In contrast to systems with 'simple' liquids, much less is known about liquid systems with compositional gradients (Thiele, Todorova & Lopez 2013). For example, sessile drops from different but completely miscible liquids with surface tensions γ_1 and γ_2 do *not* always coalesce instantaneously upon contact. After lateral contact, the drop bodies can remain separated in a temporary state of *non-coalescence*, connected through a thin liquid bridge and chase each other across their support at a constant velocity v_N (see figure 1 and Riegler & Lazar 2008; Karpitschka & Riegler 2010; Borcia & Bestehorn 2013). Recently this observation, which seemingly contradicts capillarity, has been explained. The surface tension difference $\Delta\gamma = \gamma_1 - \gamma_2$ between the drops has been identified as the reason for this behaviour (Riegler & Lazar 2008; Karpitschka & Riegler 2010, 2012). A Marangoni flow induced by $\Delta\gamma$ overrides capillarity and temporarily prevents the drop fusion (for an extended qualitative description, see supplemental material of Karpitschka & Riegler 2012). Understanding the coalescence behaviour of sessile drops of different but completely miscible liquids is important because it represents ubiquitous natural and artificial/technological cases when two bodies of different liquids attached to a solid surface come into contact. It is for instance relevant to improving a standard semiconductor surface cleaning process ('Marangoni drying', see Leenaars, Huethorst & van Oekel 1990; Marra & Huethorst 1991; Matar & Craster 2001, (this research was funded partially by industry, LAM Research AG, Austria)). Marangoni flows have also been proposed for actuation in microfluidic devices (Sellier, Nock & Verdier 2011; Sellier *et al.* 2013).

The unexpected *state* of temporary non-coalescence has already been analysed experimentally and theoretically. But the *transition* between the two modes of coalescence has not been investigated up to now. The parameters controlling the transition, how sharp it is, and the physics causing the transition are unknown. The transition and the related fundamental scientific questions are the subject of this report.

We present the first experimental evidence for a sharp threshold in the coalescence behaviour of sessile drops. As the main control parameters we identify the three-phase angles Θ and the surface tension contrast $\Delta\gamma$. The individual surface tensions (γ_1, γ_2) and liquid viscosities (η_1, η_2) barely affect the transition. The data reveal universal power laws, which couple the topographic (Θ) and the physicochemical properties $(\Delta\gamma)$ to the coalescence behaviour, and, to the transition between the two coalescence regimes. Within the lubrication approximation (Oron, Davis & Bankoff 1997), we further reduce these power laws to one single, critical Marangoni number. Additional numerical simulations reproduce characteristic features of the experimental findings. They disclose the impact of diffusive mixing on the transition between the two coalescence regimes.

2. Experimental

Experiments were performed with completely wetting liquids deposited onto the substrate as separate drops with syringes from above (figure 1). The dynamic three-phase angles $\Theta(t)$ of the continuously spreading drops are used to control the three-phase angles at the moment of mutual drop–drop contact (Ristenpart *et al.* 2006; Hernandez-Sanchez *et al.* 2012), $\Theta_{a,1}$ and $\Theta_{a,2}$, the 'adjoining three-phase angles' (see figure 1 and figure 2). $\Theta_{a,1}$ and $\Theta_{a,2}$ depend on the deposition distance/delay, the drop volumes, and the (possibly different) spreading rates. With this approach identical $(\Theta_{a,1} \approx \Theta_{a,2})$ as well as different adjoining three-phase angles $(\Theta_{a,1} \neq \Theta_{a,2})$ can be

https://doi.org/10.1017/jfm.2014.73 Published online by Cambridge University Press

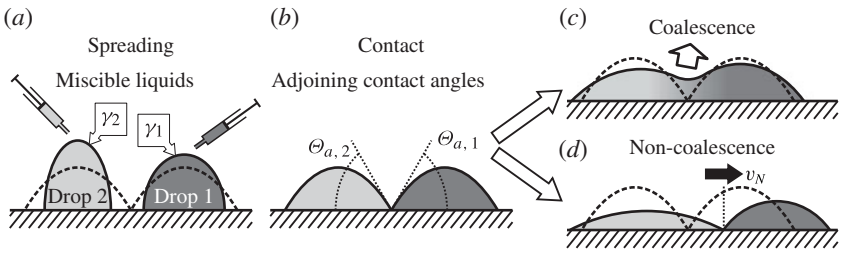


FIGURE 1. Sketch of the experimental procedure. Initial volume and distance of the two drops determine the 'adjoining' three-phase angles, $\Theta_{a,1}$ and $\Theta_{a,2}$, at which the two drops come into contact. The interplay of contact angles and surface tension contrast leads to coalescence or non-coalescence.

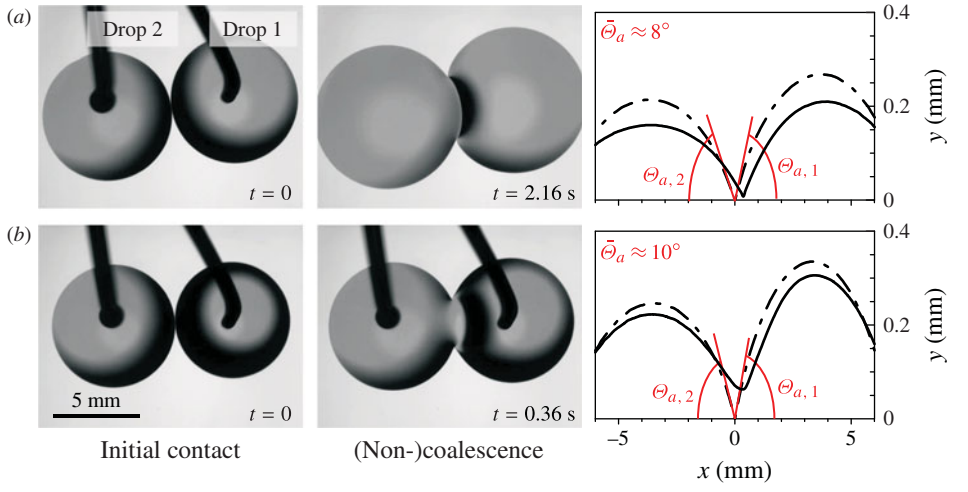


FIGURE 2. Experiments with tetradecane (drop 2) and hexadecane (drop 1). The drops in (*a*) were deposited further apart than in (*b*) leading to smaller adjoining three-phase angles. The result is non-coalescence (*a*) and immediate coalescence (*b*). This is revealed by the height profiles through the drop centres (dashed: $t = 0$; solid: $t = 2.16$ s and 0.36 s for (*a*) and (*b*), respectively). For $\overline{\Theta}_a \approx 8°$ (*a*) the connecting neck remains shallow even 2.16 s after initial contact, whereas for $\overline{\Theta}_a \approx 10°$ (*b*) the neck height has already increased substantially after 0.36 s. The syringe tips are not in contact with the drops. See online supplementary material for videos, available at http://dx.doi.org/10.1017/jfm.2014.73.

investigated for the individual liquid combinations (i.e. independently from γ_1, γ_2, $\Delta\gamma$ and the liquid viscosities η).

For millimetre-size drops gravitational effects on the initial coalescence behaviour are negligible (Ristenpart *et al.* 2006). This also holds for variations of the footprint radii/volumes.

The experiments were performed at $T = (20.0 \pm 0.5)°\,\mathrm{C}$ in a dry nitrogen atmosphere. The vapour pressures of the liquids are low. Evaporation effects can be neglected.

As described previously (Karpitschka & Riegler 2010, 2012) the coalescence behaviour was observed by video imaging from the top and the side. The three-phase angles were measured very accurately by taking both top and side aspects into account

https://doi.org/10.1017/jfm.2014.73 Published online by Cambridge University Press

(see online supplementary material available at http://dx.doi.org/10.1017/jfm.2014.73 for details). The liquids used were: (*a*) linear *n*-alkanes (C_nH_{2n+2} with $n = 13$–16), (*b*) branched alkanes, 2,6,10,14-tetramethylpentadecane ($C_{19}H_{40}$, 'Pristane') and 2,6,10,15,19,23-hexamethyltetracosane ($C_{30}H_{62}$, 'Squalane'), and (*c*) a branched alkene, 2,6,10,15,19,23-hexamethyl-2,6,10,14,18,22-tetracosahexaene ($C_{30}H_{50}$, 'Squalene'). The liquids were used as supplied (alkanes: purity >99.5%, Alfa Aesar; Pristane: purity ⩾95%, Sigma). Their surface tensions were measured to check purity. They agreed with the literature values (Wohlfarth & Wohlfahrt 1997). The substrates were piranha cleaned silicon wafers (see online supplementary material available at http://dx.doi.org/10.1017/jfm.2014.73 for details).

The experiments focus on the coalescence behaviour immediately after the moment of mutual drop–drop contact. The ongoing spreading before and after the contact has no significant impact on the initial coalescence behaviour because spreading shortly before contact is typically much slower than the topographical changes just after contact.

3. Experimental results

Figures 2(*a*) and 2(*b*) show the same pair of liquids (tetradecane and hexadecane, $\Delta\gamma \approx 0.87$ mN m^{-1}) for different three-phase angles in the moment of contact (adjoining three-phase angles $\Theta_a = \Theta(t=0)$). Experiments reveal that the coalescence behaviour is insensitive to the *individual* $\Theta_{a,1}$, $\Theta_{a,2}$ values. It is only a function of $\overline{\Theta}_a = (\Theta_{a,1} + \Theta_{a,2})/2$. The evolution of the drop height profiles for $t > 0$ reveals in figure 2(*a*) a persistently shallow neck. For $\overline{\Theta}_a \approx 8°$, the coalescence is suppressed (although $\Delta\gamma \approx 0.87$ mN m^{-1} is remarkably small). In figure 2(*b*) the neck height increases for $t > 0$ i.e. for $\overline{\Theta}_a \approx 10°$ the coalescence is instantaneous. This reveals a 'threshold' angle between temporary non-coalescence and immediate coalescence of $\overline{\Theta}_{a,t} \approx (9.0 \pm 1.0)°$.

For another case (hexadecane and pentadecane, $\Delta\gamma \approx 0.46$ mN m^{-1}) figure 3 shows the time evolution of the neck heights. The difference between the coalescence behaviour is evident for $\overline{\Theta}_{a,t} \approx (6.2 \pm 0.4)°$. This smaller $\overline{\Theta}_{a,t}$ compared to the system depicted in figure 2 correlates with a smaller $\Delta\gamma$. For $\overline{\Theta}_a > \overline{\Theta}_{a,t}$ (immediate coalescence), the Marangoni forces already lead to a decrease in the neck growth rate as compared to identical liquids (see inset in figure 3 and Hernandez-Sanchez *et al.* 2012). In contrast, for $\overline{\Theta}_a < \overline{\Theta}_{a,t}$, the neck growth is fully suppressed within experimental errors. Therefore we refer to the latter as *temporary non-coalescence*, to avoid confusion with the delaying effect of the Marangoni flow in the regime of immediate coalescence (Borcia & Bestehorn 2010).

Figure 4 shows the boundary between temporary non-coalescence and immediate coalescence as derived from many experiments with various liquid combinations performed as shown in figures 1–3. The boundary between the two regimes of coalescence is defined by the threshold average adjoining three-phase angle $\overline{\Theta}_{a,t}$. For all investigated combinations of liquids, $\overline{\Theta}_{a,t}$ scales approximately with the square root of $\Delta\gamma/\overline{\gamma}$:

$$\overline{\Theta}_{a,t} \approx \frac{180°}{\pi}(0.85 \pm 0.05)\ (\Delta\gamma/\overline{\gamma})^{0.50\pm0.02}\,. \tag{3.1}$$

The liquid viscosities varied by approximately an order of magnitude, from 2.3 mPa s (tetradecane, Wohlfarth & Wohlfahrt 2001) to 28 mPa s (Squalane, Fermeglia & Torriano 1999). The surface tensions ranged from 26.2 mN m^{-1}

https://doi.org/10.1017/jfm.2014.73 Published online by Cambridge University Press

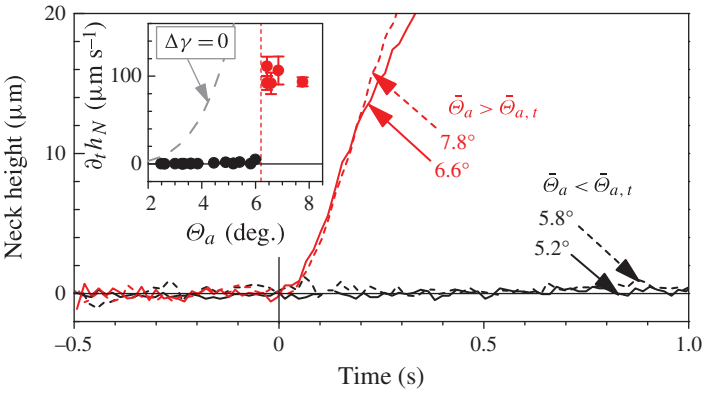


FIGURE 3. Neck height vs. time (contact at $t = 0$) for hexadecane and pentadecane drops ($\Delta\gamma \approx 0.46$ mN m^{-1}). The four experiments differ only in their $\overline{\Theta}_a$ value at $t = 0$ with a threshold angle $\overline{\Theta}_{a,t} \approx (6.2 \pm 0.4)°$. The noise/height resolution is $\approx \pm 1$ μm. Inset: Initial neck growth rate vs. $\overline{\Theta}_a$ compared to the behaviour for identical liquids (Hernandez-Sanchez *et al.* 2012) ($\Delta\gamma = 0$, dashed grey line $\propto \Theta^4$).

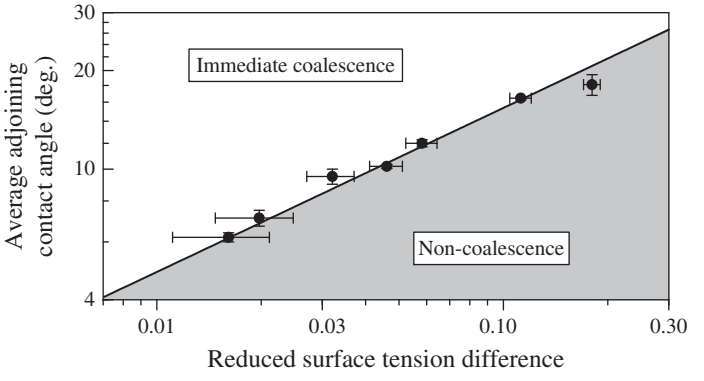


FIGURE 4. Threshold behaviour of the coalescence of drops from different, miscible liquids: Threshold average adjoining threshold three-phase angle $\overline{\Theta}_{a,t}$ vs. reduced surface tension difference $\Delta\gamma/\overline{\gamma}$ (double logarithmic plot). Drops with $\overline{\Theta}_a > \overline{\Theta}_{a,t}$, i.e. above the threshold curve, coalesce instantaneously; those with $\overline{\Theta}_a > \overline{\Theta}_{a,t}$ (below the threshold) exhibit non-coalescence. The upper and lower ends of the error bars represent the experiments within each regime that were closest to the boundary. The line is the result of the scaling (exponent) and the simulations (prefactor), and contains no fit parameter.

(Pristane, Körösi & Kováts 1981) to 31.5 mN m^{-1} (Squalene, Shrestha *et al.* 2006). In agreement with earlier observations on other liquids (Karpitschka & Riegler 2010), neither viscosities nor absolute surface tensions seemed to have a significant impact on the threshold behaviour.

4. Discussion and theoretical analysis

The theoretical description will be reduced to the symmetry (x, z)-plane of the drops (z-direction normal to the substrate, x-direction parallel to the substrate through the

https://doi.org/10.1017/jfm.2014.73 Published online by Cambridge University Press

two apices, see Ristenpart *et al.* 2006). With drop heights $h < 500$ μm, diameters 2 mm $< l <$ 10 mm, and speeds $<$mm s^{-1}, Reynolds number and aspect ratio are small. The system can be analysed in the lubrication approximation. With a surface tension gradient, the profile evolution equation reads (Oron *et al.* 1997):

$$\partial_t h = -\partial_x \left\{ \frac{1}{\eta} \left[\frac{h^3}{3} \partial_x \left(\gamma \partial_x^2 h \right) + \frac{h^2}{2} \partial_x \gamma \right] \right\}. \tag{4.1}$$

The surface tension is described by $\gamma = \gamma_2 + \Delta\gamma\,\phi$, with γ_2 the surface tension of liquid 2 and $\phi \in [0, 1]$ the local mass fraction of liquid 1 (Karpitschka & Riegler 2012). In the capillary term of (4.1) $\gamma(x)$ can be replaced by $\overline{\gamma}$ because $\Delta\gamma \ll \overline{\gamma}$: compared to the large, negative capillary pressure in the neck region, the difference in capillary pressure between the main bodies of the two drops can be neglected (Karpitschka & Riegler 2012). The viscosities of the two liquids are similar. In addition, experiments show that the difference of the viscosities does not measurably influence the transition between the coalescence modes (Karpitschka & Riegler 2010). Thus we replace $\eta(x)$ by $\overline{\eta} = (\eta_1 + \eta_2)/2$. To account for the low aspect ratio ϵ of the profiles, we scale $\xi = h/l_0$ and $\chi = \epsilon x/l_0$, where l_0 is the (vertical) length scale of the profile. We define l_0 via the drop apex heights at the moment of mutual contact (see below). The scale of the slopes in the profile at mutual drop–drop contact is given by $\overline{\Theta}_a$. Therefore we set the aspect ratio:

$$\epsilon = \overline{\Theta}_a\, \pi/180^\circ. \tag{4.2}$$

Thus, in dimensionless units, the slope $\partial_\chi \xi \lessapprox 1$. The time variable is scaled as $\tau = v_c t/l_0$, with a capillary velocity $v_c = \overline{\gamma}\epsilon^4/(3\eta)$ (Aarts, Schmidt & Lekkerkerker 2004). The evolution equation becomes

$$\partial_\tau \xi = -\partial_\chi \Big[\underbrace{\xi^3 \partial_\chi^3 \xi}_{=\Phi_C} + \underbrace{\widetilde{M} \xi^2 \partial_\chi \phi}_{=\Phi_M} \Big], \tag{4.3}$$

with an effective Marangoni number

$$\widetilde{M} = 3\Delta\gamma/(2\overline{\gamma}\epsilon^2). \tag{4.4}$$

In (4.3) Φ_C is the flow due to capillarity from both sides into the neck region. It changes sign at the neck *regardless* of the individual curvatures/surface tensions of the two main drop bodies, because the neck region is curved in the opposite direction and much more strongly than the main drop bodies. Φ_M is the Marangoni flow due to the (local) surface tension gradient. $\Phi_M > 0$ everywhere, since $\partial_\chi \phi > 0$ everywhere. Thus, Φ_M can compensate Φ_C, i.e. suppress coalescence, if Φ_M is strongest/localized to the region where $\Phi_C < 0$. As long as Φ_M can compensate Φ_C, coalescence is suppressed and the drops form a travelling wave (Karpitschka & Riegler 2012). If Φ_M cannot compensate Φ_C, immediate coalescence occurs. Φ_M scales with $\widetilde{M} \propto \Delta\gamma/(\overline{\gamma}\epsilon^2)$.

Since the typical neck heights during non-coalescence are in the μm range (for immediate coalescence, they quickly grow to much larger values, see Karpitschka & Riegler 2012; Hernandez-Sanchez *et al.* 2012), we do not include a disjoining pressure (which acts for $h \lessapprox 10$ nm, Israelachvili 2002) in our analysis. For the case here (completely wetting liquids), the disjoining pressure, in addition to capillarity, promotes coalescence during the very first moments of drop–drop contact.

https://doi.org/10.1017/jfm.2014.73 Published online by Cambridge University Press

Associating the threshold behaviour in coalescence with a universal threshold Marangoni number, $\widetilde{M}_t$, equation (4.4) implies that $\overline{\Theta}_{a,t}$ scales as follows:

$$\overline{\Theta}_{a,t} = \frac{180^\circ}{\pi}\sqrt{\frac{3\Delta\gamma}{2\widetilde{M}_t\overline{\gamma}}}. \tag{4.5}$$

This agrees with the experimental data (3.1) yielding:

$$\widetilde{M}_t \approx 2.0 \pm 0.2. \tag{4.6}$$

$\widetilde{M}_t$ marks the shift in dominance between the two flux contributions that exist if there is a (local) surface tension gradient characterized by $\Delta\gamma$ and a non-planar liquid surface characterized by $\overline{\Theta}_a$. The result of the competing contributions is either separation of the liquid bodies (Marangoni dominates, $\widetilde{M} > \widetilde{M}_t$) or their convergence (capillarity dominates, $\widetilde{M} < \widetilde{M}_t$).

5. Simulations

To gain additional insight we also performed numerical simulations. These focused in particular on $\widetilde{M}_t$, its relation to the molecular diffusivity of liquid 2 in liquid 1, D, and the category of the transition characterized by $\widetilde{M}_t$. D affects the local surface tension gradient via the local composition evolution (Karpitschka & Riegler 2012). Thus it influences the coalescence behaviour. Experimentally it is difficult to vary D independently of other system parameters. Therefore, simulations with varying D are particularly useful.

We analysed numerically (4.3) coupled to the evolution equation for ϕ (the vertically averaged mass fraction of liquid 1) in the lubrication approximation (Oron *et al.* 1997):

$$\partial_\tau(\phi\,\xi) = -\partial_\chi\left\{\phi\left[\xi^3\partial_\chi^3\xi + \widetilde{M}\xi^2\partial_\chi\phi\right] - \widetilde{D}\xi\,\partial_\chi\phi\right\}, \tag{5.1}$$

where $\widetilde{D} = 3\eta D/(l_0\overline{\gamma}\epsilon^2)$ is the scaled diffusion constant.

Except for $\widetilde{D}$, the length scale l_0 does not appear in the equations or the remaining (dimensionless) constants. Thus, the size of the drops in the simulation can be matched to any drop size in the experiments (as long as they are small enough to neglect gravity compared to capillarity), by defining l_0 appropriately. $\widetilde{D}$ was chosen to yield realistic values for D after defining l_0. In addition, $\widetilde{D}$ was varied by about an order of magnitude around that value.

The simulations started with two parabolas as the 'drops' with a scaled three-phase angle of 1 and an apex height of $\xi_{apex} = 500$ on top of a precursor film of $\xi_{precursor} = 1$. The introduction of a precursor avoids the three-phase line singularity. A series of simulations with different apex heights on the same precursor showed that for $\xi_{apex} \gtrapprox 100$, the coalescence behaviour is no longer significantly influenced by the presence of the precursor. The large height ratio of 500 between drops and precursor mimics realistic conditions (Borcia *et al.* 2012). This also implies that the 'microscopic contact angle' (determined by the slope in the inflection point near the contact line), is virtually identical to the overall aspect ratio (determined by the apex height over the footprint width) of the profile. Details on the simulation method can be found in the online supplemental material available at http://dx.doi.org/10.1017/jfm.2014.73.

https://doi.org/10.1017/jfm.2014.73 Published online by Cambridge University Press

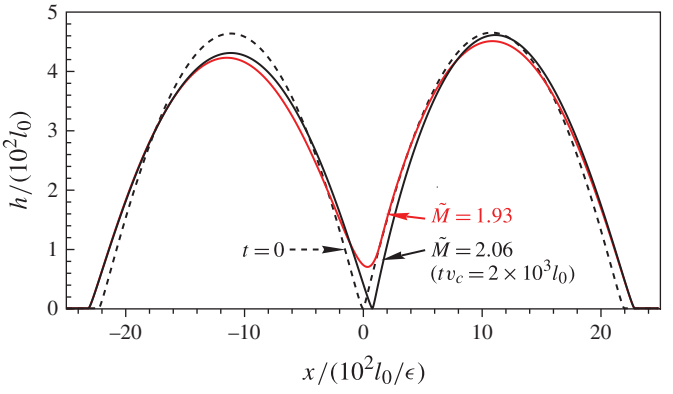


FIGURE 5. Snapshots of drop profiles during numerical simulations (see online supplementary material available at http://dx.doi.org/10.1017/jfm.2014.73 for details). Dashed: moment of drop–drop contact ($t = 0$). Solid: at later time, $t\,v_c = 2 \times 10^3 l_0$, for $\widetilde{M} < \widetilde{M}_t$ (red) and $\widetilde{M} > \widetilde{M}_t$ (black). With $l_0 = 5 \times 10^{-7}$ m, the apex heights match those from the experiments.

Figure 5 shows simulated drop profiles with $\widetilde{D} = 0.125$ and two different $\widetilde{M}$. Profiles are shown at the moment of contact ($\tau = 0$) and after contact at $\tau = 20$. The profiles at contact are nearly identical for both $\widetilde{M}$ values because $\widetilde{M}$ has only a weak impact on the spreading behaviour on the thin precursor. After contact the two cases develop very differently. For $\widetilde{M} = 1.95$, the neck height h_N grows, whereas for $\widetilde{M} = 2.12$ it remains constantly low. This means immediate coalescence and temporary non-coalescence, respectively, with $\widetilde{M}_t \approx 2$.

The simulations indicate that $\widetilde{M}_t$ weakly depends on $\widetilde{D}$ ($\propto \widetilde{D}^{1/10}$ for $5 \times 10^{-2} \leqslant \widetilde{D} \leqslant 1$, see inset of figure 6). The simulation data nicely reproduce the experimental findings depicted in figures 2 and 3. In particular, for $\widetilde{D} = 0.125$ they simulate systems with the same $\widetilde{M}_t \approx 2$. The simulations also suggest a rather sharp transition (within $\pm 5\%$ of $\widetilde{M}_t$) between the two coalescence regimes for this range of $\widetilde{D}$.

How do these findings translate into physical dimensions? For the experiments, D and its scaled equivalent $\widetilde{D}$, are not known exactly. Considering the drops in figure 2, $l_0 = 5 \times 10^{-7}$ m (matching $\xi_{apex} = 500$ to $h_A = 2.5 \times 10^{-4}$ m), $\overline{\Theta}_a = 10^\circ$ (i.e. $\epsilon = 0.175$), $\eta = 2.5 \times 10^{-3}$ Pa s, and $\overline{\gamma} = 27 \times 10^{-3}$ N m^{-1}. With these values, $v_c = 3.5 \times 10^{-3}$ m s^{-1}, and $\widetilde{D} = 0.125$ translates into $D = 6.5 \times 10^{-9}$ m^2 s^{-1}. This is a reasonable value and corroborates the validity of the simulations (see Cussler 1997). Translating the transition range of $\approx \pm 5\%$ of $\widetilde{M}_t$ into contact angles for $\Delta\gamma = 0.87$ N m^{-1} yields a transition within $\approx \pm 0.2^\circ$, which is below a reasonable measurement resolution.

A disjoining pressure would act in the range of $\lessapprox 10$ nm, which translates into $2 \times 10^{-2} l_0$. The neck height at the threshold between coalescence and non-coalescence ($t v_c \approx 2 \times 10^2 l_0$ in figure 6) is already around $2l_0$. Thus we estimate that the disjoining pressure is not relevant for the threshold, which is supported by the quantitative agreement of our simulations (without disjoining pressure) and the experimental threshold $\widetilde{M}_t$. Rather, it seems important to use a large height ratio between the drop apices and the precursor in the simulations.

https://doi.org/10.1017/jfm.2014.73 Published online by Cambridge University Press

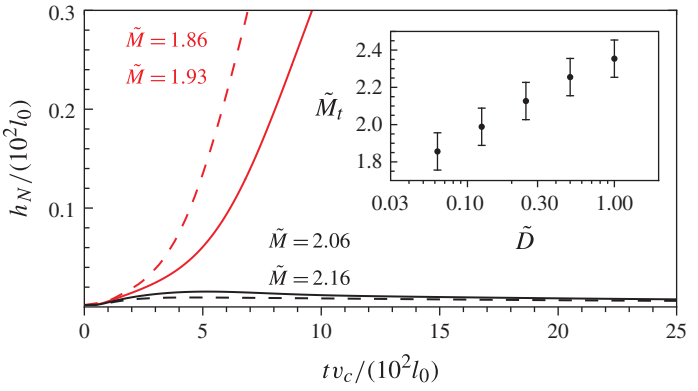


FIGURE 6. Neck height h_N vs. time for $\widetilde{M} < \widetilde{M}_t$ (red) and $\widetilde{M} > \widetilde{M}_t$ (black). The solid curves correspond to the profiles from figure 5 ($\widetilde{M} = 1.93, 2.06$). The inset shows the threshold Marangoni number $\widetilde{M}_t$ as a function of the effective diffusion constant $\widetilde{D}$.

6. Summary and conclusions

We present the first comprehensive experimental results on a sharp transition in coalescence behaviour of sessile drops of different but completely miscible liquids. A wide range of three-phase angles was investigated for different γ_1, γ_2, $\Delta\gamma$ and liquid viscosities η. The average three-phase angle $\overline{\Theta}_a$ has been identified as the main topographic control parameter. The transition between the regimes of immediate coalescence and non-coalescence is sharp with respect to the threshold three-phase angle $\overline{\Theta}_{a,t} \propto \sqrt{\Delta\gamma/\overline{\gamma}}$. For $\overline{\Theta}_a > \overline{\Theta}_{a,t}$ coalescence occurs immediately, for $\overline{\Theta}_a < \overline{\Theta}_{a,t}$ (temporary) non-coalescence is observed.

From the scaling of the lubrication equation we extract a characteristic Marangoni number $\widetilde{M} = 3\Delta\gamma/(2\overline{\gamma}(\overline{\Theta}_a\,\pi/180°)^2)$ as measure for the competition between the coalescence-promoting capillarity and the drop-separating Marangoni flow. It is the key system parameter regarding the coalescence behaviour and unifies the impact of the physicochemical liquid properties and the shape of the liquid bodies in the contact region. The experimental data for the threshold $\overline{\Theta}_{a,t}$ collapse into a single threshold Marangoni number $\widetilde{M}_t \approx 2$. This is in quantitative agreement with simulations assuming a realistic value for the diffusivity. The simulations also reveal a rather sharp boundary and that $\widetilde{M}_t$ depends on the diffusivity of liquid 2 in liquid 1.

The concepts and results are relevant in numerous cases, whenever two bulk liquid bodies (drops, films) of different composition get in contact.

Acknowledgements

We acknowledge helpful discussions with Jacco Snoeijer, Uwe Thiele, and Michael Köpf, and technical support from Ferec Liebig. We also thank H. Möhwald for scientific advice and general support. S.K. was supported by the DFG (RI529/16-1) and LAM Research AG, Austria.

Supplementary data

Supplementary data is available at http://dx.doi.org/10.1017/jfm.2014.73.

https://doi.org/10.1017/jfm.2014.73 Published online by Cambridge University Press

References

AARTS, D. G. A. L., SCHMIDT, M. & LEKKERKERKER, H. N. W. 2004 Direct visual observation of thermal capillary waves. *Science* **304**, 847–850.

BORCIA, R. & BESTEHORN, M. 2010 Different behaviors of delayed fusion between drops with miscible liquids. *Phys. Rev.* E **82**, 036312.

BORCIA, R. & BESTEHORN, M. 2013 Partial coalescence of sessile drops with different miscible liquids. *Langmuir* **29**, 4426–4429.

BORCIA, R., BORCIA, I. D. & BESTEHORN, M. 2012 Nonlinear dynamics of thin liquid films consisting of two miscible components. *Phys. Rev.* E **86**, 056319.

CASTREJÓN-PITA, J. R., KUBIAK, K. J., CASTREJÓN-PITA, A. A., WILSON, M. C. T. & HUTCHINGS, I. M. 2013 Mixing and internal dynamics of droplets impacting on a solid surface. *Phys. Rev.* E **88**, 023023.

CHRISTOPHER, G. F., BERGSTEIN, J., POON, M., NGUYEN, C. & ANNA, S. L. 2009 Coalescence and splitting of confined droplets at microfluidic junctions. *Lab on a Chip* **9**, 1102–1109.

CUSSLER, E. L. 1997 *Diffusion: Mass Transfer in Fluid Systems*. Cambridge University Press.

EDDI, A., WINKELS, K. G. & SNOEIJER, J. H. 2013 Influence of droplet geometry on the coalescence of low viscosity drops. *Phys. Rev. Lett.* **111**, 144502.

FERMEGLIA, M. & TORRIANO, G. 1999 Density, viscosity, and refractive index for binary systems of n-C16 and four nonlinear alkanes at 298.15K. *J. Chem. Engng Data* **44**, 965–969.

HANYAK, M., DARHUBER, A. A. & REN, M. S. 2011 Surfactant-induced delay of leveling of inkjet-printed patterns. *J. Appl. Phys.* **109**, 074905.

HERNANDEZ-SANCHEZ, J. F., LUBBERS, L. A., EDDI, A. & SNOEIJER, J. H. 2012 Symmetric and asymmetric coalescence of drops on a substrate. *Phys. Rev. Lett.* **109**, 184502.

IHNEN, A. C., PETROCK, A. M., CHOU, T., FUCHS, B. E. & LEE, W. Y. 2012 Organic nanocomposite structure tailored by controlling droplet coalescence during inkjet printing. *ACS Appl. Mater. Interfaces* **4**, 4691–4699.

ISRAELACHVILI, J. 2002 *Intermolecular and Surface Forces*. 2nd edn. Academic Press.

KARPITSCHKA, S. & RIEGLER, H. 2010 Quantitative experimental study on the transition between fast and delayed coalescence of sessile droplets with different but completely miscible liquids. *Langmuir* **26**, 11823–11829.

KARPITSCHKA, S. & RIEGLER, H. 2012 Non-coalescence of sessile drops from different but miscible liquids: Hydrodynamic analysis of the twin drop contour as self stabilizing, traveling wave. *Phys. Rev. Lett.* **109**, 066103.

KÖRÖSI, G. & KOVÁTS, E. SZ. 1981 Density and surface tension of 83 organic liquids. *J. Chem. Engng Data* **26**, 323–332.

LEENAARS, A. F. M., HUETHORST, J. A. M. & VAN OEKEL, J. J. 1990 Marangoni drying: a new extremely clean drying process. *Langmuir* **6**, 1701–1703.

LI, Z. G., ANDO, K., YU, J. Q., LIU, A. Q., ZHANG, J. B. & OHL, C. D. 2011 Fast on-demand droplet fusion using transient cavitation bubbles. *Lab on a Chip* **11**, 1879–1885.

MARRA, J. & HUETHORST, J. A. M. 1991 Physical principles of marangoni drying. *Langmuir* **7**, 2748–2755.

MATAR, O. K. & CRASTER, R. V. 2001 Models for marangoni drying. *Phys. Fluids* **13**, 1869–1883.

ORON, A., DAVIS, S. H. & BANKOFF, S. G. 1997 Long-scale evolution of thin liquid films. *Rev. Mod. Phys.* **69**, 931–980.

RIEGLER, H. & LAZAR, P. 2008 Delayed coalescence behavior of droplets with completely miscible liquids. *Langmuir* **24**, 6395–6398.

RISTENPART, W. D., MCCALLA, P. M., ROY, R. V. & STONE, H. A. 2006 Coalescence of spreading droplets on a wettable substrate. *Phys. Rev. Lett.* **97**, 064501.

SELLIER, M., NOCK, V., GAUBERT, C. & VERDIER, C. 2013 Droplet actuation induced by coalescence: experimental evidences and phenomenological modeling. *Eur. Phys. J. Spec. Top.* **219**, 131–141.

SELLIER, M., NOCK, V. & VERDIER, C. 2011 Self-propelling, coalescing droplets. *Intl J. Multiphase Flow* **37**, 462–468.

https://doi.org/10.1017/jfm.2014.73 Published online by Cambridge University Press

SHRESTHA, L. K., ARAMAKI, K., KATO, H., TAKASE, Y. & KUNIEDA, H. 2006 Foaming properties of monoglycerol fatty acid esters in nonpolar oil systems. *Langmuir* **22**, 8337–8345.

STRINGER, J. & DERBY, B. 2010 Formation and stability of lines produced by inkjet printing. *Langmuir* **26**, 10365–10372.

THIELE, U., TODOROVA, D. V. & LOPEZ, H. 2013 Gradient dynamics for films of mixtures and suspensions: dewetting triggered by coupled film height and concentration fluctuations. *Phys. Rev. Lett.* **111**, 117801.

WOHLFARTH, C. & WOHLFAHRT, B. 1997 *Surface Tension of Pure Liquids and Binary Liquid Mixtures* In Landolt Börnstein, IV (Physical Chemistry), vol. 16. Springer.

WOHLFARTH, C. & WOHLFAHRT, B. 2001 *Viscosity of Pure Organic Liquids and Binary Mixtures* In Landolt Börnstein, IV (Physical Chemistry), vol. 18. Springer.

https://doi.org/10.1017/jfm.2014.73 Published online by Cambridge University Press